# Very long transients, irregular firing, and chaotic dynamics in networks of randomly connected inhibitory integrate-and-fire neurons

Rüdiger Zillmer,[1,2,3] Nicolas Brunel,[1,2] and David Hansel[1,2]
[1]*Laboratoire de Neurophysique et Physiologie, Université Paris Descartes, 75270 Paris Cedex 06, France*
[2]*CNRS, UMR 8119, 45 rue des Saints Pères, 75270 Paris Cedex 06, France*
[3]*Istituto dei Sistemi Complessi, CNR via Madonna del Piano 10, I-50019 Sesto Fiorentino, Italy*
(Received 3 December 2008; revised manuscript received 22 January 2009; published 18 March 2009)

We present results of an extensive numerical study of the dynamics of networks of integrate-and-fire neurons connected randomly through inhibitory interactions. We first consider delayed interactions with infinitely fast rise and decay. Depending on the parameters, the network displays transients which are short or exponentially long in the network size. At the end of these transients, the dynamics settle on a periodic attractor. If the number of connections per neuron is large ($\sim$1000), this attractor is a cluster state with a short period. In contrast, if the number of connections per neuron is small ($\sim$100), the attractor has complex dynamics and very long period. During the long transients the neurons fire in a highly irregular manner. They can be viewed as quasistationary states in which, depending on the coupling strength, the pattern of activity is asynchronous or displays population oscillations. In the first case, the average firing rates and the variability of the single-neuron activity are well described by a mean-field theory valid in the thermodynamic limit. Bifurcations of the long transient dynamics from asynchronous to synchronous activity are also well predicted by this theory. The transient dynamics display features reminiscent of *stable chaos*. In particular, despite being linearly stable, the trajectories of the transient dynamics are destabilized by finite perturbations as small as $O(1/N)$. We further show that stable chaos is also observed for postsynaptic currents with finite decay time. However, we report in this type of network that chaotic dynamics characterized by positive Lyapunov exponents can also be observed. We show in fact that chaos occurs when the decay time of the synaptic currents is long compared to the synaptic delay, provided that the network is sufficiently large.

DOI: 10.1103/PhysRevE.79.031909 PACS number(s): 87.19.lj, 84.35.+i, 05.45.Xt

## I. INTRODUCTION

Spike trains of cortical neurons recorded *in vivo* during spontaneous as well as evoked periods of activity are highly irregular [1–6]. The strong irregularity of neuronal dynamics *in vivo* is also visible in intracellular traces which exhibit large fluctuations in membrane potentials [7,8]. This contrasts with the nearly periodic trains of action potentials recorded *in vitro* in neurons stimulated with constant or weakly noisy current (see, e.g., [9]).

*In vivo* irregular spiking in cortex is a nontrivial feature because of the large number of afferents cortical neurons receive. Indeed, assuming asynchronous firing of $K \gg 1$ presynaptic afferents, the resulting temporal fluctuations in the postsynaptic current (PSC) should be much smaller, by a factor $1/\sqrt{K}$, than the average current. Accordingly, since *in vitro* neurons fire regularly in response to constant current inputs, one would expect firing *in vivo* to be only weakly irregular. A possible explanation of the observed variability is to assume that in cortical networks excitatory and inhibitory inputs nearly balance, so that their temporal fluctuations are small compared to their means taken separately but are as large as the average total synaptic input [10–14]. In such a state the neural activity is driven mostly by the temporal fluctuation in the synaptic input rather than by their means. Hence the neural firing is irregular. The "balance of excitation and inhibition" can be rigorously defined in the thermodynamic limit in which the number of excitatory neurons, $N_E$, and the number of inhibitory neurons, $N_I$, goes to infinity. As shown in [11,12], if the connectivity $K$ is large but sparse, i.e., $1 \ll K \ll N_E, N_I$, and the coupling strength is scaled proportionally to $1/\sqrt{K}$, balanced states emerge from the collective dynamics of the network without any fine tuning of parameters. Moreover, balanced states are largely independent of single-cell intrinsic properties. In fact they can be equally found in networks of binary neurons [11,12], integrate-and-fire neurons [13–16], as well as for more realistic conductance-based dynamics [17]. Note that balanced states occur not only in excitatory-inhibitory networks, but also emerge in strongly connected purely inhibitory networks receiving strong external inputs.

An approximate self-consistent mean-field theory can be developed to study the asynchronous activity in networks of integrate-and-fire neurons in the thermodynamic limit. This theory assumes that the connectivity matrix of the neurons is random and sparse and that the interactions are delayed and of brief duration ($\delta$-function synaptic currents) [13,14]. This theory applies to the balanced excitation-inhibition regime and predicts accurately the distribution of the firing rates of the neurons as well as the coefficient of variation (CV) of their interspike intervals (ISIs). It also predicts the instabilities of the balanced state as function of the network parameters.

In contrast to the dynamics of randomly connected neurons, the dynamics of fully connected networks are in general periodic or weakly irregular. Depending on the nature of the interactions (excitatory or inhibitory), the synaptic dynamics (delay, rise, and decay time), and heterogeneities in the external inputs, these networks display diverse patterns of activity, e.g., full synchrony, cluster states, or asynchronous states (see, e.g., [18]). In particular, the patterns of syn-

 

chrony of inhibitory leaky integrate-and-fire (LIF) networks with all-to-all connectivity have been studied extensively [19–21]. When there is no delay in the synaptic transmission and the time course of the postsynaptic current is instantaneous, the network converges to a periodic splay state [22–24]. When the interactions are noninstantaneous, the network displays stable $n$-cluster states in a broad region of parameters. In these states the network splits into $n$ groups of neurons. Within each group, neurons fire in synchrony whereas a nonzero phase shift exists between groups. In particular, a one-cluster state corresponds to full synchrony. The typical number of clusters in such states increases linearly with the inverse of the delay [21]. In all these states the neurons fire periodically or close to periodically, unless strong noise is present in the external input [19].

To understand better how randomness in the connectivity induces irregular spiking, Zillmer *et al.* [22] recently investigated the dynamics of finite-size networks of inhibitory integrate-and-fire neurons with weakly diluted connectivity and instantaneous $\delta$-function synaptic interactions (no delay). The networks they considered had small to moderate sizes (up to $N=200$ neurons). They found that at sufficiently large time the dynamics always reaches a state of periodic activity in which neurons fire in a phase-locked manner. However, the transient dynamics as well as the time needed to reach these states depend on the coupling strength (normalized to $N$). For weak coupling the transients are short, with a duration of $O(N)$. In contrast, for sufficiently strong coupling the convergence to the periodic dynamics can be extremely slow with a transient duration that is exponentially large in the network size. They also found that the dynamics during these long transient are irregular but nonchaotic since the maximum Lyapunov exponent (LE) is always negative. In fact, they showed that the transient dynamics is reminiscent of those observed in coupled map lattices in the regime of stable chaos (see e.g., [25]). Similar results were obtained by Jahnke *et al.* [26] for delayed $\delta$-function synapses and substantially more diluted connectivity than in [22]. They also provided an analytical argument showing the stability of any dynamical trajectory.

The results of Zillmer *et al.* and Jahnke *et al.* suggest that, depending on the time scale of the observation, finite-size networks of inhibitory randomly connected neurons behave either like infinitely large sparsely connected networks or like fully connected networks. They also suggest that when the size of the network is increased the thermodynamic limit behavior is reached through the divergence of the transient behavior. Our goal in the present paper is to clarify further the relationship between the finite-size transient dynamics of sparsely connected networks and their dynamics in the thermodynamic limit. We also aim at investigating whether truly chaotic states can also be observed in such networks. We define the model we investigate and we summarize previous findings regarding its dynamical properties in Sec. II. In Sec. III the different dynamical regimes exhibited by the model when the connectivity is large ($\sim$1000 synapses per neuron) and the neurons interact via $\delta$-function synapses are described. Transients with duration exponentially growing with the system size during which the neurons fire irregularly before the dynamics collapses to periodic states are studied in Sec. IV. Section V shows that when the connectivity is small ($\sim$100) the period of the dynamics to which the long transients collapse is exponentially large in the network size. In Sec. VI we show that networks with synapses with noninstantaneous decay may exhibit chaotic states, characterized by positive Lyapunov exponents, if the network is sufficiently large. We conclude by summarizing the results and raising some open issues.

## II. DEFINITION OF THE MODEL AND MEAN-FIELD APPROACH

### A. Model

We consider a network on $N$ LIF neurons, coupled via inhibitory interactions. The membrane potentials $V_i, i=1,\ldots,N$ satisfy the equation

$$\tau \dot{V}_i = I_{\text{ext}} - V_i + I_i^{\text{rec}} \tag{1}$$

supplemented by the condition that whenever $V_i$ reaches a threshold $V_t$, the neuron fires an action potential and $V_i$ is reset to $V_r$. In Eq. (1) $\tau$ is the membrane time constant of the neuron, assumed to be identical for all the cells, $I_{\text{ext}}$ is a time-independent homogeneous background external current representing inputs from neurons not explicitly described in the model, and $I_i^{\text{rec}}$ is the synaptic current that neuron $i$ receives from other neurons in the network due to the recurrent interactions ($I_{\text{ext}}$ and $I_i^{\text{rec}}$ are normalized to the neuronal membrane resistance). The recurrent current is given by

$$I_i^{\text{rec}} = \tau \sum_{j=1}^{N} \frac{J_{ij}}{K} \sum_m \alpha(t - t_j^{(m)} - D), \tag{2}$$

where $\alpha(t)$ describes the time course of the PSC induced by a single presynaptic spike and $t_j^{(m)}$ is the $m$th spike fired by neuron $j$. The function $\alpha(t)$ is normalized so that $\int \alpha(t)dt = 1$. The synaptic delay is denoted by $D$. The network connectivity matrix $J_{ij}$ is drawn randomly under the constraint that neurons receive exactly $K$ inputs. We set $J_{ij}=J$ whenever a synaptic connection exists from neuron $j$ to neuron $i$, and $J_{ij}=0$ otherwise.

The present study focuses on the case of inhibitory interactions, i.e., $J<0$, and we study the dynamics of the network as a function of $I_{\text{ext}}>V_t$, $J$, $K$, and $N$. The delay is taken to be $D=2$ ms, unless specified otherwise. The PSC time course is given by $\alpha(t)=\delta(t)$ (called $\delta$-PSC throughout the paper) except in Sec. VI where we consider the more realistic form

$$\alpha(t) = \frac{\Theta(t)}{\tau_d - \tau_r}(e^{-t/\tau_d} - e^{-t/\tau_r}) \tag{3}$$

that depends on the rise time $\tau_r$ and the decay time $\tau_d$ and where $\Theta(t)$ denotes the Heaviside function. Throughout the study we assume fixed single-neuron parameters: $\tau=20$ ms, $V_t=20$ mV, and $V_r=10$ mV (see, e.g., [9]).

As outlined in Appendix A, the dynamics of the network [Eqs. (1) and (2)] are equivalently described by a discrete-time map. Iterating numerically this map provides us with an efficient way to investigate the dynamical properties of large networks with up to $N=10\,000$ neurons and connectivity as large as $K=1000$.

In the following, $T_{\mathrm{ISI}}$ denotes the ISI of a single neuron and $t_{\mathrm{ISI}}$ the time interval between two successive action potentials *in the network*. States in which neurons fire periodically can be described in terms of a set of phase variables, $\phi_i(t)$, defined as the duration elapsed at time $t$ since the last spike fired by neuron $i$, normalized to the period of firing.

### B. Mean-field approach

Under the assumptions that neurons fire as Poisson processes, that individual connection strengths are small compared to the threshold, and that PSCs have $\delta$ functions profile, the synaptic inputs to the neurons can be modeled as white noise with a mean and a variance determined self-consistently by the dynamics of the network [13]. In this mean-field approach, the dynamics of the membrane potential of individual neurons follow a diffusion process,

$$\tau \dot{V}_i = I_{\mathrm{ext}} - V_i + \tau J R(t-D) + \tau J \sqrt{\frac{R(t-D)}{K}} \xi_i(t), \qquad (4)$$

where $\langle \xi(t)\xi(t') \rangle = \delta(t-t')$ and $R(t)$ is the instantaneous network activity (number of neurons firing between $t$ and $t+\Delta t$, divided by $N\Delta t$, in the small $\Delta t$ limit). Since fluctuations become uncorrelated from neuron to neuron when $K/N \to 0$, Eq. (4) can be transformed into a Fokker-Planck equation describing the temporal evolution of the probability distribution function of the membrane potentials. The membrane potential distribution in the asynchronous state of the network is the stationary solution of this Fokker-Planck equation. In this state the population activity is constant in time and single cells fire in a highly irregular fashion. The mean-field equations allow one to compute the average firing rate of the neurons and CV of their spike interval distribution. Furthermore, the stability of the stationary solution and the conditions for the emergence of collective oscillations can be determined by studying the Fokker-Planck operator linearized around this solution. One finds that when the inhibitory coupling is below a critical value, the asynchronous state is stable. When the inhibitory coupling is above this critical value the network goes to a synchronous state in which population oscillation emerges, while single cells keep firing in a highly irregular fashion. The critical coupling strength where the instability occurs depends on the delay $D$ as well as on the external drive [13]. The population oscillations are induced by the interplay between the negative feedback due to the recurrent interactions and the delay in its transmission. It can be shown that the period of the emerging collective oscillation is $\sim D$ when $D \ll \tau_m$.

Note that the mean-field approach assumes an infinitely large network. Moreover, in the absence of external noise [as in Eq. (1)] the noise in the synaptic input to the neurons is a consequence of the random sparse connectivity and it is generated in a self-consistent fashion by the irregular dynamics of the network. Hence, this noise disappears if the system settles on a periodic orbit in which single neurons have regular periodic firing patterns.

## III. DYNAMICS OF DILUTED NETWORKS WITH LARGE $K=1000$

In this section we present results obtained in numerical simulations of the LIF inhibitory network [Eqs. (1)–(3)] with $N=5000, K=1000$. The postsynaptic currents are modeled as a delayed $\delta$ function. We study the dynamics of the network as a function of the external drive $I_{\mathrm{ext}}$ and the strength of the couplings $J$. All the numerical simulations described in this section have a duration $t_{\max} < 10$ min.

### A. Firing patterns in simulations with random initial conditions for the membrane potentials

For initial conditions of $V_i$ drawn independently at random from a uniform distribution on $[V_r, V_t]$, our simulations show two qualitatively different regimes, depending on the values of the external current $I_{\mathrm{ext}}$ and the coupling strength $J$. When $I_{\mathrm{ext}}$ is larger than some critical value $I_c(J,D)$, which increases with $J$ and decreases with $D$, the network settles after a rapid transient, typically shorter than 2 s, in a state of periodic firing with a period $T$ equal to the single-neuron ISI, $T_{\mathrm{ISI}}$. In this state the neurons are arranged in smeared clusters [27] with all the neurons in a given cluster firing within a time window of a size of the order of $D$ [see the inset of Fig. 2(b)]. The number of clusters depends on the initial conditions and varies in a range that depends on the delay $D$. For instance, for $D=2$ ms we observe states with two to five clusters, depending on the initial condition.

In contrast, the neurons fire in a nonperiodic and irregular fashion throughout the simulation when $I_{\mathrm{ext}} < I_c(J,D)$. More precisely, in agreement with the predictions of the mean-field theory sketched above, we find two types of irregular states. For a sufficiently small drive, $I_{\mathrm{ext}} < I_{\mathrm{as}}(J,D)$, the network is in an asynchronous state, whereas for $I_{\mathrm{as}}(J,D) < I_{\mathrm{ext}} < I_c(J,D)$ the population activity is synchronous. Synchronous oscillations are for instance observed for $I_{\mathrm{ext}}=21$ mV, $J=-50$ mV, and $D=2$ ms. This is illustrated in Fig. 1(a) where the autocorrelation (AC) of the population-averaged neuronal firing rate $R(t)$ is plotted. This figure shows that the period of the oscillations is $\approx 4D$ in agreement with the mean-field prediction [13]. The damping in the oscillations is a finite-size effect: the damping time constant increases by a factor of $\approx 1.5$ if the network size is doubled [triangles in Fig. 1(a)]. These oscillations occur at the population level, while the single-neuron activity is highly irregular. The distribution of the single-neuron ISIs depends on both $I_{\mathrm{ext}}$ and $J$, and the average CV increases with $J$ and decreases with $I_{\mathrm{ext}}$. For $I_{\mathrm{ext}}$ and $J$ such that the network is well in the synchronous irregular region, the ISI distribution is broad but displays multiple peaks that are integer multiples of the population oscillation period. This is shown in Fig. 1(b) for $I_{\mathrm{ext}}=25$ mV and $J=-50$ mV. In contrast, for a lower current value, $I_{\mathrm{ext}}=22$ mV, the peaks in the ISI distribution are no longer present. At large ISI the distribution displays an exponential decay. Although the network activity displays synchronous collective oscillations for these parameters, their amplitude is too small for the multiple peaks to appear in the ISI distribution.

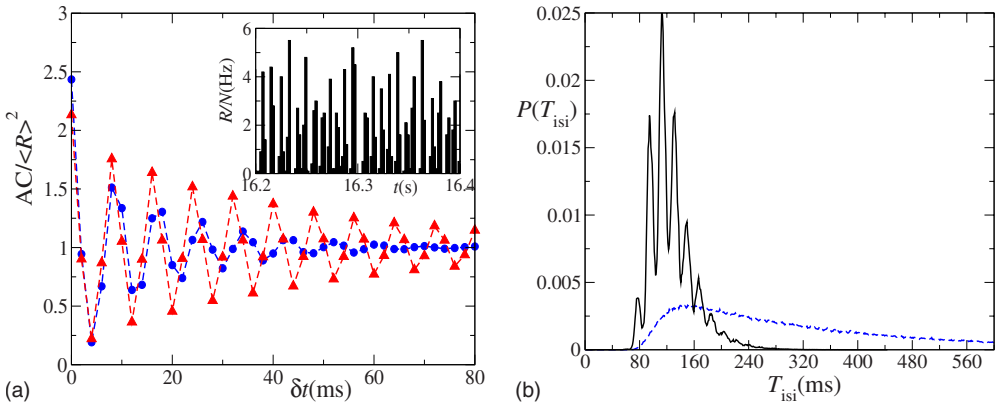


FIG. 1. (Color online) (a) The autocorrelation of the activity normalized to the time averaged activity of the network $[R(t)]$ for $N=5000$ (blue bullets) and $N=10\,000$ (red triangles); $I_{\mathrm{ext}}=21$ mV, $J=-50$ mV, $K=1000$. The inset shows a snapshot of the activity for $N=5000$. (b) The ISI distribution for $N=5000$, $K=1000$, $J=-50$ mV, $I_{\mathrm{ext}}=21$ mV (blue dashed line), and $I_{\mathrm{ext}}=25$ mV (black solid line).

### B. Dynamics of the network for initial conditions close to a cluster state

In contrast to the behavior found in simulations with random initial conditions, we find that if the network is initialized close to a cluster configuration it is always driven toward a smeared cluster state. For example, for the same parameters as in Fig. 1(a), the network is driven toward a smeared two-cluster state when it is initialized near such a state, even though for these parameters random conditions lead to irregular firing. However, sufficiently strong perturbation of the network, settled in such smeared two-cluster states, drive it away toward an irregular firing state. This happens for instance in the simulations depicted in Fig. 2, where after $t=0.6$ s the state of the network is perturbed each time a neuron fires by adding to the membrane potentials of all neurons an independent and identically distributed random number chosen according to a uniform distribution of width $1.7\times10^{-6}$ mV. These perturbations are much smaller than the typical potential difference of neurons close to the threshold $\sim10^{-4}$ mV, such that their effect is similar to that of time-continuous noise. We checked that, once the system has reached the irregular state, it remains there (for times up to $t_{\mathrm{max}}=10$ min) even after the noise has been switched off. A similar behavior is observed for different parameter values, regardless of whether the irregular state is synchronous or asynchronous. Thus, the network displays bistability between regular periodic smeared cluster states and synchronous or asynchronous irregular firing.

The phase diagram plotted in Fig. 3 summarizes the results we have described in this section. In the gray area, confined by the numerically obtained border (full circles), the network displays periodic or irregular firing state, depending on initial conditions. The coefficient of variation $(C_V)$ of single-neuron ISI in the irregular state increases as the external current is reduced for fixed $J$, thus assuming values $C_V>0.8$ below the dashed line in the phase diagram. Finally, the solid red line corresponds to the transition from asynchronous irregular firing to synchronous irregular firing as predicted by mean-field theory, in good agreement with our simulation results.

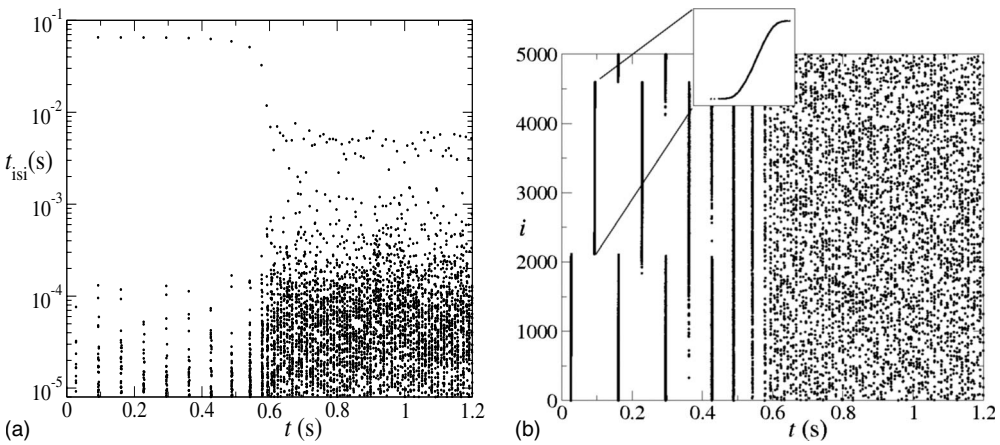


FIG. 2. Transition from cluster to irregular dynamics induced by external perturbations. $N=5000, K=1000, I_{\mathrm{ext}}=21$ mV, $J=-50$ mV. The network has been initialized in a two-cluster periodic state. For $0<t<0.6$ s the dynamics was perturbed as described in the text. The sudden transition to irregular dynamics is clearly visible. (a) The network ISI, $t_{\mathrm{ISI}}$, vs time. (b) Raster plot of the network activity. Dots represent the firing of the neurons labeled by the index $i$. The transition to the irregular dynamics when the accumulated perturbations exceed a certain threshold is clearly visible. The inset shows a zoom of a smeared cluster.

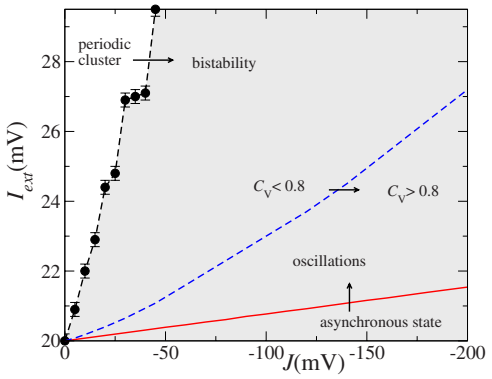


FIG. 3. (Color online) Phase diagram of the network for $N=5000, K=1000$. The domain in which stable periodic and irregular dynamics coexist is indicated in gray. See details in text.

We have treated the delay here as a fixed parameter (2 ms). Increasing the delay has the following effects: the region in which irregular transients are observed shrinks; the region in which this transient dynamics is asynchronous also shrinks, as predicted by mean-field theory [13]. Further, for long enough delays, the periodic state is always a one-cluster state, consistent with [21].

## IV. LONG TRANSIENTS TO PERIODIC STATES IN FINITE NETWORKS

### A. Irregular firing is a transient state but is "stationary" over long times

In this section we show that the irregular firing states, found in our simulations of the network with $N \geq 5000$ neurons, are in fact quasistationary states in which the dynamics, started from random initial conditions, remain transient for a duration which is exponentially large in $N$. For $N=5000$ the transient duration is on an "astronomical" time scale. However, if the system size is not that large, an abrupt switch from irregular firing to a smeared cluster state can actually be observed after a long transient.

This switching phenomenon is demonstrated in Fig. 4(a), for $N=1650$, and values of $J$ and $I_{\text{ext}}$ for which the mean-field theory predicts a stable asynchronous state in the thermodynamic limit. Initialized with random initial conditions, the network remains in the irregular state until $t \approx 463$ s, where it suddenly switches to a two-cluster state with periodic firing. Remarkably, until the abrupt switching, the transient exhibits all the characteristics of a stationary state. To show this, we computed the ISI distribution over sliding windows of $O(10\,000)$ firing events. This allows us to estimate a time-dependent average ISI, $\langle T_{\text{ISI}} \rangle(t)$, as well as a time-dependent coefficient of variation $C_V(t)$. The results, plotted in Fig. 4(b), show that both quantities remain essentially constant during the transient until the moment of the switching to the periodic cluster state, where suddenly $C_V(t) \to 0, \langle T_{\text{ISI}} \rangle(t) \to T$. Thus, one can meaningfully speak of a quasistationary irregular dynamical state that coexists with periodic cluster states. Remarkably, the observed irregular transients resemble the stationary states of the network, predicted by the mean-field theory in the sparse connectivity limit $K/N \to 0$, not only qualitatively but also quantitatively. For instance, in the case depicted in Fig. 4(b), the average $T_{\text{ISI}}$ and the $C_V$ of the ISI distribution are close to the values of 0.67 s and 0.85, respectively, predicted by the mean-field theory for the sparsely connected network ($K/N \ll 1$) with the same synaptic strength and current values, although here $K/N=0.61$. As a matter of fact, the small deviation of the numerical $T_{\text{ISI}}$ and $C_V$ from the mean-field results can be partly explained by a finite-size effect due to the usage of sliding windows of finite width for the computation of these quantities.

In order to compute the transient duration $T_{\text{tr}}$, an algorithm has been employed that searches for the first repetition (within a reasonable resolution $\varepsilon < \approx 10^{-10}$) of the membrane potential values: $\max_i |V_i(T_{\text{tr}}+T) - V_i(T_{\text{tr}})| < \varepsilon$, where $i = 1, \ldots, N$. (cf. [22]). The results obtained with a fixed number of connections, $K=1000$, various sizes of the network, and several values of $I_{\text{ext}}$ and $J$ are summarized in Fig. 5. In particular, the circles correspond to the same values of $I_{\text{ext}}$ and $J$ as in Fig. 4 and network sizes in the range $N = 1100-1650$. These results indicate clearly that the transient diverges exponentially with $N$. We also computed the period

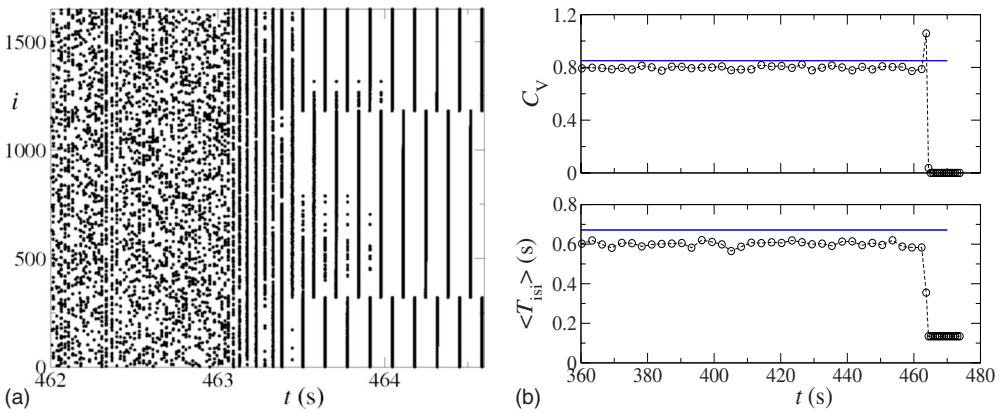


FIG. 4. (Color online) Collapse to periodic two-cluster state for $K=1000, N=1650, J=-50$ mV, $I_{\text{ext}}=21$ mV. (a) Raster plot. (b) The single-neuron ISI averaged over all the neurons, $\langle T_{\text{ISI}} \rangle$, and the average $C_V$, as function of time during the simulation depicted in (a). The solid blue lines indicate the mean-field prediction for the irregular state.

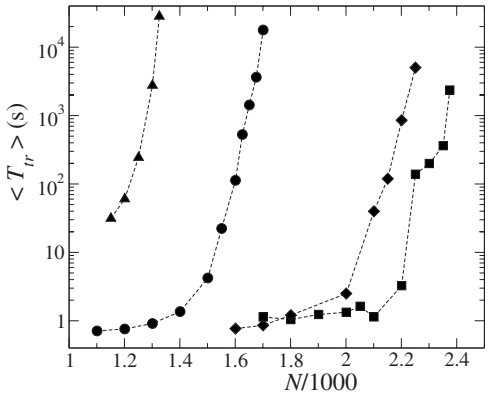


FIG. 5. The average transient duration vs $N$ for $K=1000$. Circles: $J=-50$ mV, $I_{\text{ext}}=21$ mV, squares: $J=-50$ mV, $I_{\text{ext}}=25$ mV, diamonds: $J=-150$ mV, $I_{\text{ext}}=26$ mV, and triangles: $J=-200$ mV, $I_{\text{ext}}=21$ mV. $T_{\text{tr}}$ is averaged over ten random network configurations and initial conditions of $V_i$, except for $J=-50$ mV, $I_{\text{ext}}=25$ mV for which the average is over four configurations and initial conditions.

$T$ of the firing of the neurons after the network has switched to the cluster state. In contrast to the transient duration, $T$ coincides with the single-neuron ISI of the periodic attractor and thus depends only weakly on $N$ with values close to $T \sim 100$ ms (figure not shown).

### B. Dynamical stability of irregular firing states

To analyze further the irregular dynamics we computed the largest Lyapunov exponent $\Lambda$ of the very long transient dynamics as explained in Appendix B. Note that the zero Lyapunov exponent corresponding to perturbations oriented along the trajectory itself has been removed by the adoption of the discrete-time mapping.

The maximum Lyapunov exponent for $K=1000$ and $I_{\text{ext}}=21$ mV is plotted in Fig. 6(a) as a function of $J$ for $N=5000$ (triangles) and $N=1650$ (squares). These results show that $\Lambda$ remains negative in the domain explored, including the case $J=-50$ that is considered in Figs. 2 and 4. Note also that the $C_V$ of the single-neuron ISIs [black points in Fig. 6(a)] increases monotonically with $J$ and exceeds 0.8 for $J<-40$ mV. Quite surprisingly, $C_V$, and hence the irregularity of the spike trains, increases with *decreasing* LE for $J>-90$ mV.

These results show that the quasistationary state observed during the transient is stable vis-a-vis infinitesimally small perturbations. We tested subsequently the stability of this state with respect to perturbations of the potentials on the order of $\sim N^{-1}$ by measuring the distance

$$D_P(t) = \frac{1}{N}\sum_{i=1}^{N} |V_i'(t) - V_i(t)|$$

between the trajectory $V_i(t), i=1,\ldots,N$ of the system starting with some initial conditions and a perturbed one, $V_i'(t)$, obtained from the same initial conditions except that the indices of the two neurons closest to threshold have been swapped. We found that in roughly 50% of the cases such perturbations that affect initially only two neurons, eventually spread over the whole network, leading the system to a state of irregular firing that is locally extremely different from the unperturbed one. An example is shown in Fig. 6(b), where the distance $D_P(t)$ is plotted after a swap of two neurons at $t=0$. It shows how linear stability initially attempts to suppress the perturbation (note the logarithmic scale of the vertical axis) but that eventually $D_P(t)$ increases and converges to $D_P \approx 0.76$ mV. Interestingly, this value is very close to the average distance between two uncorrelated network states, $D_{P,\text{MF}}=0.75$ mV, computed analytically from the stationary distribution of membrane potentials in the framework of the mean-field theory (see Appendix C). We observe similar behavior for other finite perturbations on the order of $\sim N^{-1}$.

The transient quasistationary and locally stable nonchaotic states of irregular firing displayed by our network are reminiscent of stable chaotic states [22,28] observed in coupled map lattices in which irregular local dynamics persist over times that are exponential or supraexponential in the size of the network. A characteristic property of stable chaotic states is the fact that they are stable against infinitesimally small perturbation on the dynamical variables but un-

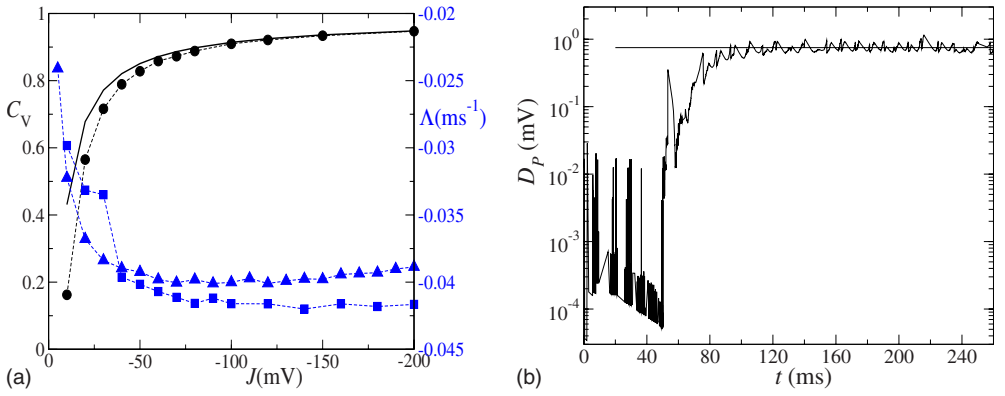


FIG. 6. (Color online) Transient dynamics for $K=1000, I_{\text{ext}}=21$ mV. (a) The average $C_V$ of single-neuron ISIs (circles, left ordinate) and the Lyapunov exponent (right ordinate, blue squares: $N=1650$ and blue triangles: $N=5000$) are plotted vs $J$. The solid line shows the mean-field prediction. (b) Distance vs time after a finite perturbation at $t=0$; $J=-50$ mV. The solid line shows the mean-field prediction.

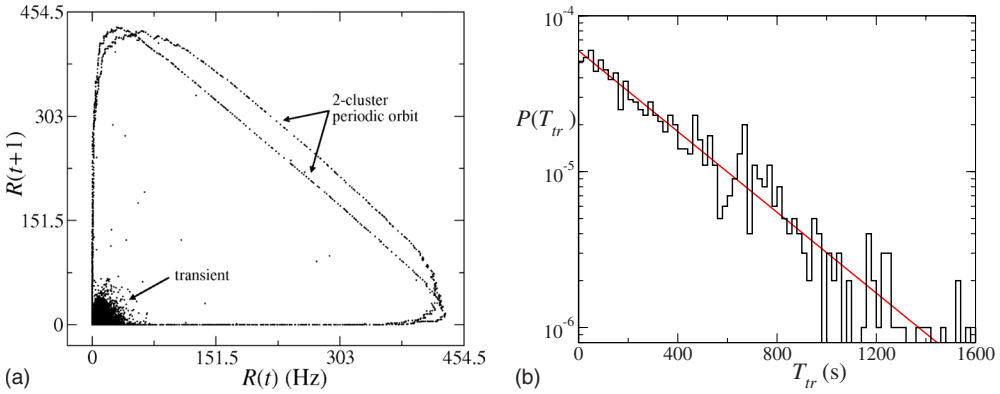


FIG. 7. (Color online) Transitions from irregular state to cluster states in a network with $N=1650, K=1000, J=-50$ mV, $I_{\text{ext}}=21$ mV. (a) Two-dimensional delay plot of the activity during the convergence to a periodic two-cluster state. (b) The distribution of transient durations $T_{\text{tr}}$, computed for 1000 different random initial conditions. The solid red line shows an exponential fit.

stable against perturbations which are small but finite, on the order of $1/N$. Consequently, the dynamics in a stable chaotic state look very irregular although the Lyapunov spectrum computed on the time scale of the persistence of the state is negative.

### C. Properties of the transient termination

In the cluster states, which the network reaches at very long time, the activity consists of short temporal windows in which large fractions of neurons fire almost simultaneously separated by long time intervals during which the network is quiescent. As a result, the temporal modulation of the averaged firing rate $R(t)$ is large, with instantaneous frequencies reaching values of several hundreds of Hz. In contrast, during the irregular transient state the temporal modulations of the activity have a small amplitude. These temporal fluctuations of the activity are partly due to a finite-size noise that, according to the mean-field theory, has a variance on the order of $\eta \sim 1/\sqrt{N}$ [13]. Subsequently, although these fluctuations are small and in fact vanish in the thermodynamic limit, their effects in a large but finite network can accumulate over sufficiently long time to drive the network away from the irregular state. When the accumulated effect of $\eta(t)$ exceeds a certain threshold $F$, the network may reach the basin of attraction of a periodic cluster state, whereupon it collapses rapidly to that state. The time this process takes on average corresponds to the average transient duration $\langle T_{\text{tr}} \rangle$. Note that the finite-size noise $\eta(t)$ is self-generated by the dynamics in the irregular state, and that once the network has escaped from this state, the fluctuations vanish. Hence the transition between the irregular state and the cluster states is strongly asymmetric: once the network has switched to the latter state it stays there.

This qualitative description of the escape process is supported by the results depicted in Fig. 7. The delay plot in Fig. 7(a) can be seen as an attractor reconstruction of a two-dimensional activity dynamics (amplitude and phase). It shows the qualitative difference between transient and periodic dynamics with respect to the existence of an internally generated noise. This suggests that the transition from transient irregular states to a periodic attractor can be viewed as a stochastic escape time problem, with a barrier $F$ and a noise $\eta \sim 1/\sqrt{N}$. In the weak-noise limit the escape time is expected to grow exponentially [29,30], i.e., $\langle T_{\text{tr}} \rangle \sim \exp(\alpha N)$. This argumentation qualitatively explains the observed divergence with the network size of the transient duration, averaged over random initial conditions (see Fig. 5). It also predicts an exponential distribution of the transient durations. We have checked the latter for a network of size $N=1650$, for which the periodic orbits are still numerically accessible and the distribution of transient durations can be obtained. The results depicted in Fig. 7(b) show that the prediction is indeed verified. The theoretical determination of the threshold $F$ and the exponent $\alpha$ would involve a nonlinear mean-field analysis of finite-size effects, which is beyond the scope of this paper.

## V. DEPENDENCE OF THE ASYMPTOTIC ATTRACTORS AND TRANSIENT DURATIONS ON THE NUMBER OF CONNECTIONS PER NEURON

The results we have presented so far concern networks with the same number of connections per neurons, $K=1000$. We now discuss, without intending to be exhaustive, what happens if one changes $K$.

Our numerical simulations reveal that long transients are observed also for small values of $K \sim O(10)$. However, which such small values of $K$, not only the transients but also the period of the attractor to which the network finally collapses have a very long duration. This is shown in Fig. 8(a) for different values of $K$ and $N$. In fact, we find the period of the attractor and the transient duration to be of the same order, i.e., both increase exponentially as functions of $N$. At some critical value, $K=K_c(N)$, a transition occurs between attractors with long periodic orbit and attractors with short periods $\sim 100$ ms, with the latter being almost insensitive to $N$ and $K$ [see Fig. 8(b)].

The long periodic orbits for small $K$ exhibit complex dynamics which are indistinguishable from the transient state on short time scales. This is depicted in Fig. 9(a). Further evidence is given by the time-dependent $C_V$ [see Fig. 9(b)] of a single neuron (different neurons exhibit similar, but not

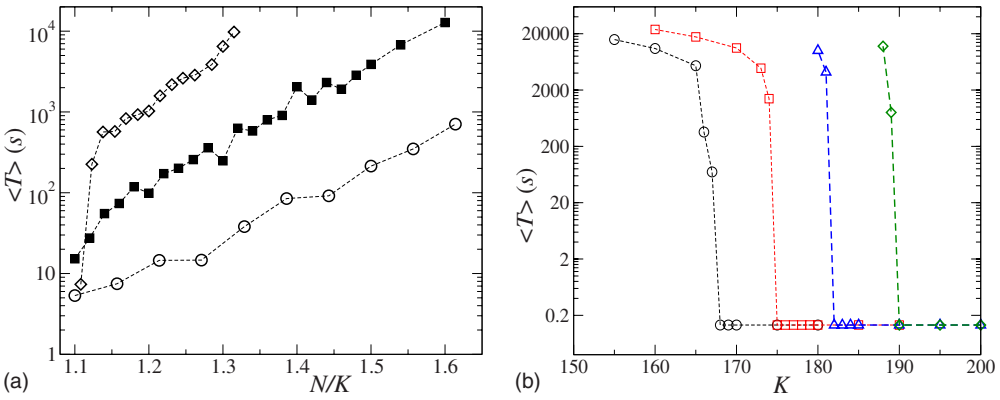


FIG. 8. (Color online) Network with small number of connections; $J=-50$ mV, $I_{\mathrm{ext}}=21$ mV. (a) The average period of the asymptotic attractor vs $N/K$ for $K=70$ (empty circles), $K=100$ (full squares), and $K=130$ (diamonds). (b) The period of the attractor, averaged over ten random network realizations and initial conditions as function of $K$ for $N=190$ (black circles), $N=200$ (red squares), $N=210$ (blue triangles), and $N=220$ (green diamonds). For $K=K_c(N)$, the period collapses to $T=134$ ms. $T$ has been averaged over ten random network realizations and initial distributions of the $V_i$.

equal, ISI patterns) that stays close to 0.8 during transient and periodic dynamics. Note that here $C_V$ of the ISI distribution fluctuates around the same value during the long transient and on the asymptotic periodic attractor. This is in contrast with the observation for $K>K_c$ (see Fig. 4). Interestingly, in this situation the mean and $C_V$ of the ISI distribution are close to the mean-field theory prediction, during the transient and on the periodic states.

We have performed numerical simulations to estimate the average transient durations for various values of $K$ and $N$. The results are summarized in Fig. 10(a), where the isolines of the transient duration are displayed in the $K$-$N$ plane. In this plane, constant dilutions ($K \propto N$) correspond to straight lines with slopes larger than unity. The two regimes for small and large $K$ are reflected in the behavior of the isolines. For small $K$ the isolines approach the diagonal, $N=K$, when $K$ is increased, thereby reducing their mutual distances. For a certain number of connections, $K_{\mathrm{max}}$, that depends on the respective network size $N$, this behavior is reversed and the isolines start to depart from the diagonal.

Increasing $N$ at a fixed $K$ gives rise to exponentially increasing transients everywhere in the $K$-$N$ plane, with an exponent that depends on $K$. For large $K$ and $N$ the isolines bend upwards with local slopes larger than 1 (see inset of Fig. 10). This implies that the exponentially large transient durations depend on $N$ and $K$ via $\beta(K)N/K$, where $\beta(K)$ depends weakly on $K$.

Consider now a straight line in the $K$-$N$ plane with $N=aK$, $a>1$. For small values of $K$ this line crosses the isolines, which is tantamount to exponentially increasing transients. However, because the isolines bend upward for large $K$, the line $N=aK$ finally crosses the isolines in the opposite direction, i.e., the transients decay for $K \gg 1$. Thus, the transient duration assumes a maximum at $K_{\mathrm{max}}$, which is demonstrated in Fig. 10(b). Our results indicate that the value $K_{\mathrm{max}}$, at which $T_{\mathrm{tr}}$ assumes a maximum, is very close to the value $K_c$ where the transition between long and short periodic attractors occurs. A possible reason for the decay of $T_{\mathrm{tr}}$ for large $K$ is the decrease in the size of the fluctuations of the synaptic inputs to the neurons, which for $N \gg 1$ scale as $\sim 1/\sqrt{K}$ [cf. Eq. (4)].

It would be interesting to characterize the transition which occurs at $K=K_c(N)$ in more detail, with the focus on its behavior at large $N$. For instance, our results do not allow us to

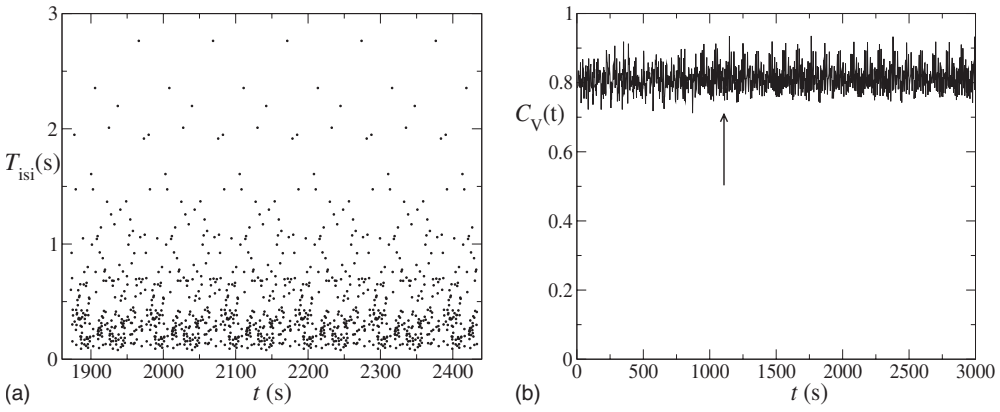


FIG. 9. Periodic attractor with a very long period for $K=100, N=130$. Other parameters are $J=-50$ mV, $I_{\mathrm{ext}}=21$ mV. (a) The ISI of a sample neuron vs time on the long periodic orbit. The period is $T \approx 103$ s. (b) The $C_V$ of the single-neuron ISIs vs time (cf. Fig. 4). The transition to the periodic dynamics is marked by the arrow.

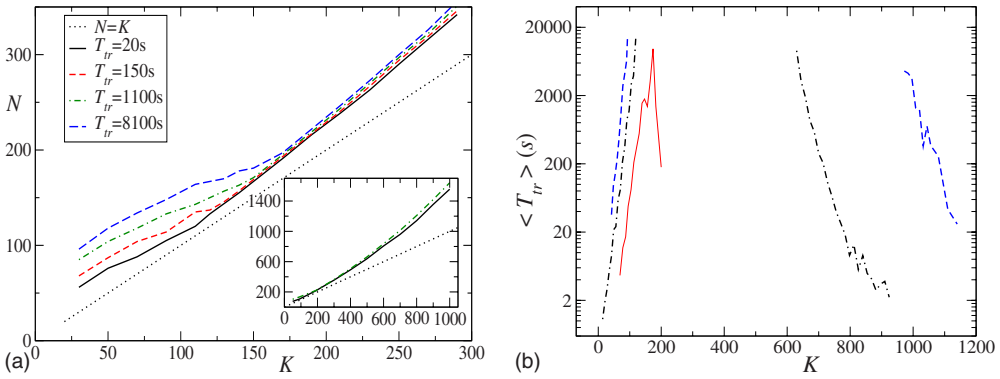


FIG. 10. (Color online) (a) Isolines of transient durations in the $N$-$K$ plane for $J=-50$ mV, $I_{\mathrm{ext}}=21$ mV. In the inset the range of $K$ and $N$ has been expanded. Dotted line: $K=N$. (b) The average transient duration vs $K$ for $N=1.67K$ (blue dashed line), $N=1.43K$ (black dotted-dashed line), and $N=1.15K$ (red solid line).

exclude the possibility that $K_c(N)$ for $N\to\infty$ saturates at a finite value. Unfortunately, the necessary computational effort is formidable due to the exponentially long time scales involved.

## VI. DYNAMICS WITH POSTSYNAPTIC CURRENTS OF FINITE WIDTH

### A. Long irregular transients

For PSCs with finite rise and decay times [see Eq. (3)], the dynamics can again be mapped onto a discrete-time map, analogous to the procedure for $\delta$-PSCs. However, the interspike interval $t_{\mathrm{ISI}}(n)$ is now given by a transcendental equation that has to be solved iteratively at each integration step. This slows down the numerical computations considerably, and hence we restrict the numerical analysis to (presumably) significant samples of the parameter space. Regarding the shape of the PSC we considered two cases: (i) a symmetric shape, $\tau_d=\tau_r=\tau_\alpha$, and (ii) a sharp rise and slow decay ($\tau_r=0, \tau_d>0$). We found that for both time courses the behavior resembles the one observed for $\delta$-PSCs. Indeed, the simulations confirm the existence of periodic cluster states as well as transients exponentially long in the size of the network. During the transients the dynamics is highly irregular, with values of the CV close to the ones we found for the $\delta$-PSC limit.

We illustrate these conclusions with specific examples in Fig. 11. In Fig. 11(a) the average transient duration for $\tau_\alpha=0.5$ ms and $D=2$ ms is compared with the case of $\delta$-function PSC. Apart from a shift of the curve to higher values of $N$, the duration grows exponentially with $N$ with roughly the same exponent for both cases. The results depicted in Fig. 11(b) confirm that the single-neuron ISI statistics is almost unaffected by the presence of a finite time constant $\tau_\alpha=0.5$ ms (compare solid black line and black circles). Also the LE, shown in the same figure, stays distinctly negative, with some positive (upward) shift compared to the $\delta$-PSC case. The periodic dynamics that is reached after the transient is again characterized by cluster states. Thus, for short PSCs with $\tau_\alpha \lesssim D$ we recover the dynamical regimes as described in Sec. IV.

### B. Chaotic dynamics with broad PSCs and short delays

Remarkably, and in contrast with the case of $\delta$-PSCs, we also observed a truly chaotic region with positive LE when the PSC time constant is large enough. We present here the

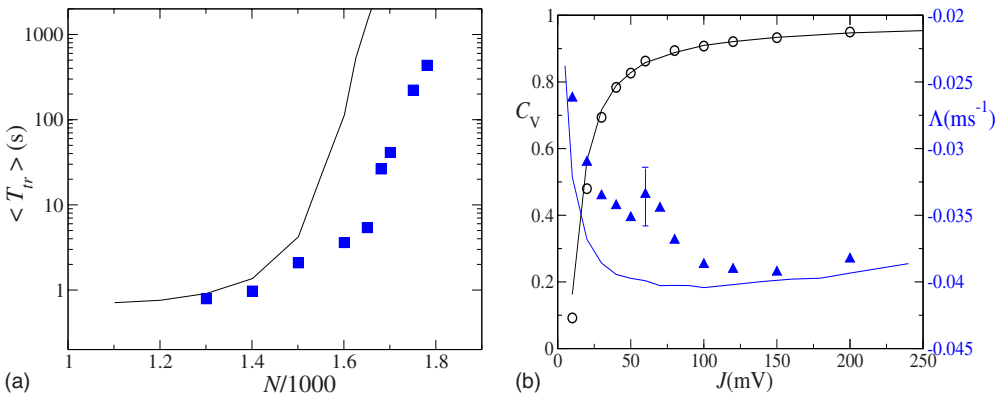


FIG. 11. (Color online) Irregular long transients for PSCs with finite width. Parameters are $K=1000, J=-50$ mV, $I_{\mathrm{ext}}=21$ mV, $\tau_\alpha=0.5$ ms. The solid lines show the $\delta$-PSC case. (a) The transient duration averaged over five random initial conditions for different values of $N$ (blue squares). (b) Population-averaged $C_V$ of the single-neuron ISIs (left ordinate, circles) and the largest Lyapunov exponent (right ordinate, blue triangles) vs $J$ for $N=4000$.

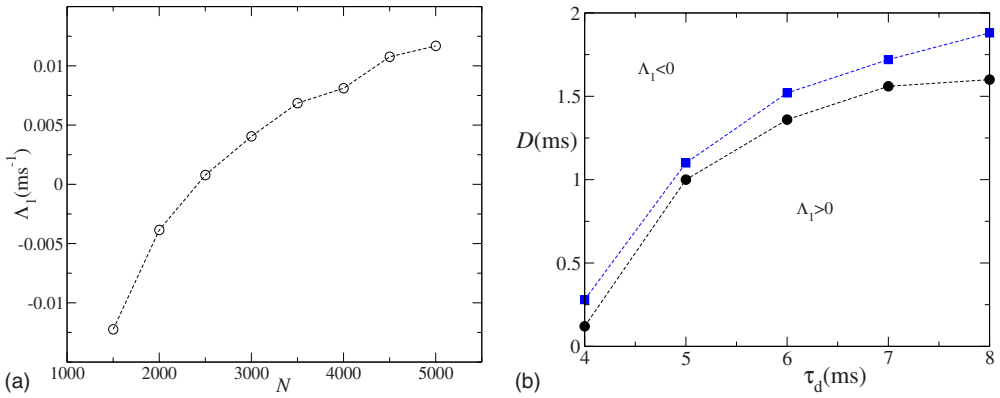


FIG. 12. (Color online) Chaotic dynamics with finite-width PSCs. Parameters are $K=1000, J=-50$ mV, $I_{\text{ext}}=21$ mV. (a) The largest Lyapunov exponent vs $N$ for $\tau_d=8$ ms and $D=1$ ms. (b) Diagram showing the chaotic and nonchaotic phases for $N=4000$ (black circles) and $N=4500$ (blue squares).

results for zero rise time, $\tau_r=0$, and different delays $D \leq 2$ ms. Similar results are found for symmetric PSCs, $\tau_d = \tau_r$.

As shown in Fig. 12(a), for $\tau_d=8$ ms and $D=1$ ms the largest Lyapunov exponent $\Lambda_1$ increases with growing system size. It becomes positive when $N \approx 2500$. We have numerically estimated $\Lambda_1$ for different values of the decay time constant $\tau_d$ and delay $D$. We found that it is positive in a broad range of these parameters. This is depicted in a phase diagram in Fig. 12(b) for two values of $N$. The border corresponding to $\Lambda_1=0$ shifts upward when $N$ is increased, thus enlarging the region where the dynamics is chaotic. Simulations performed for network sizes up to $N=6000$ suggest that the transition location converges to some limiting line in the large $N$ limit.

The variation of the first three Lyapunov exponents along a vertical cut through the $\tau_d$-$D$ plane at $\tau_d=8$ ms is plotted in Fig. 13. The results show that the Lyapunov spectrum starts to expand and to increase toward higher values when the delay is decreased beyond $D=D_c \approx 3$ ms. Upon further reduction in $D$, the exponents $\Lambda_1, \Lambda_2$ successively cross zero to become positive. We tested that the Lyapunov spectrum does not degenerate for $D>3$ ms; however, the separation of nearby exponents is small and on the order of $N^{-1}$. This

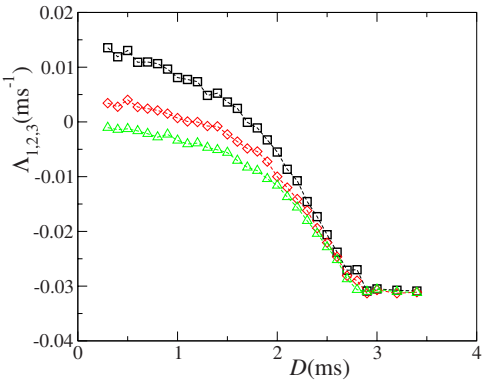


FIG. 13. (Color online) The three largest Lyapunov exponents $\Lambda_1$ (squares), $\Lambda_2$ (red diamonds), and $\Lambda_3$ (green triangles) vs delay $D$ for $N=4000$. Parameters are $K=1000, J=-50$ mV, $I_{\text{ext}}=21$ mV, $\tau_d=8$ ms.

suggests that there is a qualitative change in the dynamics before the onset of chaos, namely, when the spectrum starts to expand at $D_c$. Indeed, we find that $D_c$ decreases and finally vanishes when $\tau_d$ is decreased, i.e., the expansion of the spectrum is not present in the $\delta$-PSC limit.

These results are consistent with the fact that we did not observe true chaos with $\delta$ PSCs. In fact, chaos appears when the time constant of the postsynaptic current is increased beyond a critical value that depends on the delay $D$. The emergence of a chaotic region requires also a sufficiently large degree of connectivity. For instance, tests for varying numbers of connections per neuron revealed that, for the parameters of Fig. 12(b), the chaotic region disappears when $K$ falls below $K \lessapprox 400$.

Despite the observed chaotic dynamics when starting from random initial conditions, there might still exist stable periodic orbits with a finite basin of attraction. Indeed, we observe the simple one cluster (all neurons fire simultaneously) to remain stable. On the other hand, we find that the two-cluster state always destabilizes upon entering the chaotic region. We never observed the chaotic state to collapse on a periodic solution. However, we cannot exclude this possibility on the basis of our numerical simulations because the time scale over which a collapse may in fact occur can be exceedingly long.

## VII. CONCLUSION

In this paper, we have reconsidered the dynamics of randomly connected integrate-and-fire neurons coupled through inhibition, with the focus on the transient dynamics when the size of the networks is finite. When the decay of the synapses following a spike is much faster than the synaptic delay and the number of connections per neurons is large, the network dynamics converge rapidly to periodic cluster states if the synaptic coupling is weak. In contrast, when the coupling is strong the transient dynamics are exponentially long in the network size and exhibit stable chaos. During the transients, the dynamics are locally stable with respect to sufficiently small perturbations, as shown by previous studies in similar networks [22,26]. However, they appear to be "chaotic" in the sense that the firing patterns are highly irregular. This

irregularity is intimately connected with a high sensitivity of the dynamics against finite perturbations. In previous works [22,25] strong nonlinearities in the phase space have been identified as a necessary, but not sufficient, condition for the emergence of this type of chaotic dynamics. In the present case, the combined effect of the nonlinearity introduced by the reset of the membrane potential at the threshold and the asymmetric interactions due to the random connectivity gives rise to configurations that are sensitive against finite perturbations. However, an analytical derivation of the parameter values, where the effect of the nonlinearities is sufficiently strong to sustain the irregular transient dynamics is still an open problem. Note that convergence to a periodic state was shown analytically by Jin [31] in a network without synaptic delays. Further, it should be noticed that exponentially long transients have also been observed in diluted excitatory networks [32].

We showed that, during the long transients, the firing rate and the irregular firing patterns are as predicted by the mean-field theory of the asynchronous state in infinitely large sparse networks [13]. As the synaptic delay is varied, the asynchronous transient dynamics undergo bifurcations to population oscillations that are also predicted by the mean-field theory [13]. We have also provided a theoretical argument explaining the abrupt termination of the transient. The escape from the transient state is driven by the noise generated by the network dynamics due to the randomness of the connectivity and the finite size of the network. This argument allows us to account for the exponential distribution of the transient duration, observed in the simulations when the initial conditions of the network are changed.

Our simulations indicate that the duration of the transients depends mostly on $N$ and $K$ through the ratio $N/K$. However, the periodic states reached after the long transients strongly depend on $K$. When the number of connections per neuron is large ($K \gtrapprox 200$ for the parameters investigated in this paper), the state which is reached is a smeared cluster state with a short period that is comparable to the interspike interval of single neurons. In contrast, when $K$ is small ($K < \sim 100$) the period of the asymptotic state increases exponentially with the system size $N$. Interestingly, in these periodic states the firing patterns of the neurons are very irregular on a short time scale, which does not depend on the system size. Understanding the origin of these two qualitatively different regimes and how the transition between them occurs as $K$ is varied remains a topic for future work. It should be noted that periodic states with periods exponentially long in the network size have been found in networks of binary neurons with random asymmetric connectivity [33].

An important question is whether the stability of precise spike time trajectories can be observed in real neuronal networks, in which many sources of noise are present. The fact that perturbations on the order of $1/N$ destabilize such trajectories seems to indicate that, with realistic levels of noise, stable trajectories can be observed only in very small networks. Furthermore, we find that the transient duration for a given initial condition varies strongly for different noise realizations. For larger noise amplitudes, the periodic states destabilize and the behavior is governed by the irregular dynamics, which can be either asynchronous or synchronous [13]. This suggests that the periodic solutions play no role for the behavior of large noisy systems. For small networks that exhibit a rich variety of periodic configurations one might speculate whether the apparent coexistence of irregular and periodic dynamics is of relevance for information processing purposes. We leave this issue as an open problem for future research.

Chaos has been shown to exist in spatially structured networks [34,35]. In the present paper, we report that unstructured randomly connected integrate-and-fire networks of finite size can also exhibit chaotic states. We found that when the synaptic delay is small and the decay time of the synaptic currents is beyond some critical value, the dynamics have one or several strictly positive Lyapunov exponents. Relying on our numerical simulations for different values of the network size, we conjecture that the maximum Lyapunov exponent remains strictly positive also in the thermodynamic limit, and therefore that the dynamics is also chaotic in that limit. For the same parameters and finite systems we find that the synchronized one-cluster state remains stable. Hence, although we never observed the chaotic dynamics to collapse onto periodic solutions, we cannot exclude this possibility in finite systems. The nature of the relationship between the chaoticity and the temporal correlations in the synaptic currents induced by the noninstantaneous decay of the synapses remains to be determined.

Our results, as well as those of [22,26], concern networks of inhibitory integrate-and-fire neurons with discontinuous dynamics and with synaptic dynamics that are discontinuous or have discontinuous derivatives. Therefore, one may wonder whether similar behavior can be found in networks with more realistic and smoother neuronal and synaptic dynamics. Our preliminary results indicate that long transients exhibiting irregular dynamics are also observed in networks of Hodgkin-Huxley conductance-based inhibitory neurons (not shown). A systematic study of the properties of these long transients requires formidable computational power. We leave this investigation for future work.

## APPENDIX A: EVENT-DRIVEN MAP

Dynamics (1) can be mapped onto a discrete-time map, which we demonstrate in the following for the case of delta PSCs (see also [22,35]). First let us simplify Eq. (1) by using the rescaled variables

$$\tilde{t} = \frac{t}{\tau}, \quad \tilde{V}_i = \frac{I_{\text{ext}} - V_i}{I_{\text{ext}} - V_t}, \quad \tilde{D} = \frac{D}{\tau}, \quad \tilde{J} = \frac{J}{I_{\text{ext}} - V_t},$$

$$\tilde{V}_t = 1, \quad \tilde{V}_r = \frac{I_{\text{ext}} - V_r}{I_{\text{ext}} - V_t}.$$

Thus the temporal evolution transforms into

$$\dot{\tilde{V}}_i = -\tilde{V}_i + \sum_{j=1}^{N} \frac{\tilde{J}_{ij}}{K} \sum_m \delta(\tilde{t} - \tilde{t}_j^{(m)} - \tilde{D}), \quad V_i \in (1, \infty). \tag{A1}$$

Let $\tilde{V}_i(n)$ denote the membrane potential of the $i$th neuron and $\delta t_j^{(m)}(n) = \tilde{D} - \tilde{t} + \tilde{t}_j^{(m)}$, $\delta t_j^{(m)}(n) > 0$ denote the "waiting

time" of a spike to induce a postsynaptic current, both immediately after the $n$th event (firing or PSC induction). One can easily infer from Eq. (A1) that the time interval needed by the $i$th neuron to reach the firing threshold in the absence of spikes is $\delta t_i(n)=\ln \tilde{V}_i(n)$. The first step is to find the minimum of the time intervals, $\Delta t(n)=\min\{\delta t_j^{(m)}(n), \delta t_i(n)\}$. Now there are two cases to be considered.

(i) *PSC induction.* Let the shortest time interval be $\delta t_l^{(p)}(n)$, which sets the integration time step of the map, i.e., $\Delta t(n)=\delta t_l^{(p)}(n)$. By now including the effect of the next spike, the network dynamics can be transformed into a discrete map as follows:

$$\tilde{V}_i(n+1)=\frac{\tilde{V}_i(n)}{\exp[\Delta t(n)]}+\frac{\tilde{J}_{ik}}{K}, \tag{A2a}$$

$$\delta t_j^{(m)}(n+1)=\delta t_j^{(m)}(n)-\Delta t(n). \tag{A2b}$$

As a matter of course, $\delta t_l^{(p)}(n)$ is removed from the stack.

(ii) *Firing.* Let the shortest time interval be $\delta t_k(n)$. Now the dynamics is given by an exponential relaxation or time shift, respectively, and a new spike, $q$, is added to the system,

$$\tilde{V}_k(n+1)=\tilde{V}_r, \tag{A3a}$$

$$\tilde{V}_i(n+1)=\frac{\tilde{V}_i(n)}{\tilde{V}_k(n)}, \tag{A3b}$$

$$\delta t_j^{(m)}(n+1)=\delta t_j^{(m)}(n)-\Delta t(n), \tag{A3c}$$

$$\delta t_k^{(q)}=\tilde{D}. \tag{A3d}$$

The process can be iterated by finding the minimum among $\{\delta t_j^{(m)}(n+1), \delta t_i(n+1)\}$ and so on. Therefore, $\Delta t(n)$ represents the time interval between the $n$th an the $(n+1)$th spike; following the standard notation, it will be denoted with $t_{\mathrm{ISI}}(n)$. On the other hand, $T_{\mathrm{ISI}}(n)$ denotes the time elapsed between the $(n+1)$th spike and the previous spike emitted by the *same* neuron.

## APPENDIX B: LINEARIZED DYNAMICS AND LYAPUNOV EXPONENT

For the following we assume that the membrane potentials (measured at discrete time steps) of different neurons do not coincide. Due to the random topology of the synaptic matrix this is guaranteed, except for the trivial one-cluster state where all neurons are initialized at the same value. We denote infinitesimal perturbations of the potentials $\tilde{V}_i$ by $\tilde{w}_i$ and perturbations of $\delta t_j^{(m)}$ as $\delta\tau_j^{(m)}$. Adopting the terminology of Appendix A the linearized dynamics is given as follows:

(i) PSC induction:

$$\tilde{w}_i(n+1)=\frac{\tilde{w}_i(n)}{\exp[\Delta t(n)]}-\frac{\tilde{V}_i(n)}{\exp[\Delta t(n)]}\delta\tau_l^{(p)}(n), \tag{B1a}$$

$$\delta\tau_j^{(m)}(n+1)=\delta\tau_j^{(m)}(n)-\delta\tau_l^{(p)}(n). \tag{B1b}$$

(ii) Firing:

$$\tilde{w}_k(n+1)=0, \quad \delta\tau_k^{(q)}=0, \tag{B2a}$$

$$\tilde{w}_i(n+1)=\frac{\tilde{w}_i(n)}{\tilde{V}_k(n)}-\frac{\tilde{V}_i(n)}{\tilde{V}_k(n)^2}\tilde{w}_k(n), \tag{B2b}$$

$$\delta\tau_j^{(m)}(n+1)=\delta\tau_j^{(m)}(n)-\frac{\tilde{w}_k(n)}{\tilde{V}_k(n)}. \tag{B2c}$$

For the calculation of Lyapunov exponents we iterate the original as well as a set of linearized equations and reorthonormalize the perturbation vectors periodically using a modified Gram-Schmidt algorithm (see [36] and references therein).

## APPENDIX C: MEAN-FIELD CALCULATION OF THE DISTANCE BETWEEN UNCORRELATED STATES

When PSCs are delta functions, in the diffusion approximation, the distribution of membrane potentials in an asynchronous network state is given by

$$P(V)=\frac{2R_0\tau}{\sigma}\exp\left(-\frac{(V-\mu_0)^2}{\sigma_0^2}\right)\int_{(V-\mu_0)/\sigma_0}^{(V_t-\mu_0)/\sigma_0}\times\Theta\left(u-\frac{(V_r-\mu_0)^2}{\sigma_0^2}\right)\exp(u^2)du, \tag{C1}$$

where

$$R_0=\frac{1}{\sqrt{\pi}\tau\displaystyle\int_{(V_r-\mu_0)/\sigma_0}^{(V_t-\mu_0)/\sigma_0}\exp(u^2)[1+\mathrm{erf}(u)]} \tag{C2}$$

is the mean firing rate, $\mu_0=I_{\mathrm{ext}}+JR_0\tau$ is the mean input to the cell, and $\sigma_0=\sqrt{J^2R_0\tau/K}$. The distance between uncorrelated states is

$$D=\int dVdW|V-W|P(V)P(W), \tag{C3}$$

where $P(V)$ is the stationary distribution of membrane potentials [Eq. (C1)].

[1] B. D. Burns and A. C. Webb, Proc. R. Soc. London, Ser. B **194**, 211 (1976).
[2] R. J. Douglas, K. Martin, and D. Whitbridge, J. Physiol. (London) **440**, 659 (1991).
[3] W. R. Softky and C. Koch, J. Neurosci. **13**, 334 (1993).
[4] W. Bair, C. Koch, W. Newsome, and K. Britten, J. Neurosci. **14**, 2870 (1994).
[5] G. Holt, W. Softky, C. Koch, and R. Douglas, J. Neurophysiol. **75**, 1806 (1996).
[6] A. Compte, C. Constantinidis, J. Tegnér, S. Raghavachari, M. Chafee, P. S. Goldman-Rakic, and X.-J. Wang, J. Neurophysiol. **90**, 3441 (2003).
[7] J. S. Anderson, I. Lampl, D. C. Gillespie, and D. Ferster, Science **290**, 1968 (2000).
[8] C. Monier, F. Chavane, P. Baudot, L. J. Graham, and Y. Fregnac, Neuron **37**, 663 (2003).
[9] D. McCormick, B. Connors, J. Lighthall, and D. Prince, J. Neurophysiol. **54**, 782 (1985).
[10] M. V. Tsodyks and T. Sejnowski, Network **6**, 111 (1995).
[11] C. van Vreeswijk, Phys. Rev. E **54**, 5522 (1996).
[12] C. van Vreeswijk and H. Sompolinsky, Neural Comput. **10**, 1321 (1998).
[13] N. Brunel and V. Hakim, Neural Comput. **11**, 1621 (1999).
[14] N. Brunel, J. Comput. Neurosci. **8**, 183 (2000).
[15] C. van Vreeswijk and H. Sompolinsky, in *Methods and Models in Neurophysics*, Lecture Notes of the Les Houches Summer School 2003, Vol. Session 80, edited by C. Chow, B. Gutkin, D. Hansel, C. Meunier, and J. Dalibard (Elsevier, New York, 2005).
[16] A. Lerchner, G. Sterner, J. Hertz, and M. Ahmadi, Network **17**, 131 (2006).
[17] T. Z. Lauritzen, Master's thesis, Niels Bohr Institute, Copenhagen, Denmark, 1998 (unpublished).
[18] G. Mato, in *Methods and Models in Neurophysics*, Lecture Notes of the Les Houches Summer School 2003, Vol. Session 80, edited by C. Chow, B. Gutkin, D. Hansel, C. Meunier, and J. Dalibard (Elsevier, New York, 2005).
[19] N. Brunel and D. Hansel, Neural Comput. **18**, 1066 (2006).
[20] L. F. Abbott and C. van Vreeswijk, Phys. Rev. E **48**, 1483 (1993).
[21] U. Ernst, K. Pawelzik, and T. Geisel, Phys. Rev. Lett. **74**, 1570 (1995).
[22] R. Zillmer, R. Livi, A. Politi, and A. Torcini, Phys. Rev. E **74**, 036203 (2006).
[23] S. Nichols and K. Wiesenfeld, Phys. Rev. A **45**, 8430 (1992).
[24] S. Strogatz and R. Mirollo, Phys. Rev. E **47**, 220 (1993).
[25] A. Politi, R. Livi, G. L. Oppo, and R. Kapral, Europhys. Lett. **22**, 571 (1993).
[26] S. Jahnke, R. M. Memmesheimer, and M. Timme, Phys. Rev. Lett. **100**, 048102 (2008).
[27] D. Golomb and D. Hansel, Neural Comput. **12**, 1095 (2000).
[28] R. Bonaccini and A. Politi, Physica D **103**, 362 (1997).
[29] H. A. Kramers, Physica (Amsterdam) **7**, 284 (1940).
[30] R. S. Maier and D. L. Stein, Phys. Rev. E **48**, 931 (1993).
[31] D. Z. Jin, Phys. Rev. Lett. **89**, 208102 (2002).
[32] A. Zumdieck, M. Timme, T. Geisel, and F. Wolf, Phys. Rev. Lett. **93**, 244103 (2004).
[33] U. Bastolla and G. Parisi, J. Phys. A **30**, 5613 (1997).
[34] A. Roxin, N. Brunel, and D. Hansel, Phys. Rev. Lett. **94**, 238103 (2005).
[35] P. C. Bressloff and S. Coombes, Neural Comput. **12**, 91 (2000).
[36] K. Geist, U. Parlitz, and W. Lauterborn, Prog. Theor. Phys. **83**, 875 (1990).